

Effects of obliquity and water vapor/trace gas greenhouses in the early martian climate

Michael A. Mischna,¹ Victor Baker,² Ralph Milliken,³ Mark Richardson,⁴ and Christopher Lee⁴

Received 11 July 2012; revised 15 November 2012; accepted 18 January 2013; published 31 March 2013.

[1] We explore possible mechanisms for the generation of warm, wet climates on early Mars as a result of greenhouse warming by both water vapor and periodic volcanic trace emissions. The presence of both water vapor (a strong greenhouse gas) and other trace greenhouse gases (such as SO₂) in a predominantly CO₂ atmosphere may act, under certain conditions, to elevate surface temperatures above the freezing point of liquid water, at least episodically. Variations in obliquity are explored to investigate whether these periodic variations in insolation at Mars can broaden the regions or seasons where warm temperatures can exist. We use the Mars Weather Research and Forecasting general circulation model to perform several simulations of the conditions of the early martian atmosphere containing these gases and find global temperatures to be cooler than the elevated levels suggested by at least one recent study by *Johnson et al.* (2008). While achieving temperatures above 273 K globally remains challenging, the additional warming by greenhouse gases under certain obliquity states can permit for widespread seasonally warm conditions, which can help to explain the presence of fluvial surface features (e.g., valley networks) and hydrous minerals of post-Noachian age, a period when alternate methods do not convincingly explain the sustainability of liquid water. Furthermore, we find that global warming can be achieved with the presence of a darker surface globally, which is consistent with both widespread exposure of unweathered basaltic bedrock or the presence of a large surface ocean or sea.

Citation: Mischna, M. A., V. Baker, R. Milliken, M. Richardson, and C. Lee (2013), Effects of obliquity and water vapor/trace gas greenhouses in the early martian climate, *J. Geophys. Res. Planets*, 118, 560–576, doi:10.1002/jgre.20054.

1. Introduction

[2] There is widespread support for the argument that during the earliest period of martian history, the Noachian (>3.7 Ga), the planet was substantially warmer and wetter than at present day [e.g., *Pollack et al.*, 1987; *Craddock and Howard*, 2002; *Hoke and Hynek*, 2009]. The mechanism by which the climate of Mars was maintained in a possible “warm, wet” state, however, remains unclear.

[3] Many of these arguments invoke thicker and, hence, warmer CO₂-based atmospheres in order to achieve surface temperatures at or above the melting point of water. These

early atmospheres would have subsequently eroded to space or otherwise diminished. Varied attempts to explain surface conditions at or above these temperatures through enhanced greenhouse warming in the atmosphere have all suffered from complications, especially under the reduced solar luminosity of the young Sun [*Gough*, 1981; *Sackmann and Boothroyd*, 2003] (resulting in the so-called “faint young Sun” paradox). A thick (multibar) CO₂ atmosphere appears to be incapable of providing the required warming [*Kasting*, 1991; *Wordsworth et al.*, 2013]. Additional contributions from a range of atmospheric gases and aerosols have been suggested, but these, too, suffer from seemingly fatal flaws that have precluded their widespread acceptance as key components of the early martian climate. Gases such as ammonia and methane [*Kuhn and Atreya*, 1979; *Kasting*, 1982] have short photochemical lifetimes, which require steady replenishment to maintain any extended greenhouse role. Organic hazes [*Sagan and Chyba*, 1997] are unlikely to be produced in the oxidizing martian atmosphere, whereas sulfur dioxide [*Postawko and Kuhn*, 1986; *Yung et al.*, 1997] is highly soluble and may precipitate quickly. The presence of IR-scattering CO₂ ice clouds [*Forget and Pierrehumbert*, 1997; *Mischna et al.*, 2000; *Forget et al.*, 2013] have likewise been proposed, but the scenario requires a large fractional cloud cover that is not expected from the dynamics of the early

¹Jet Propulsion Laboratory, California Institute of Technology, Pasadena, California, USA.

²Department of Planetary Sciences, Lunar and Planetary Laboratory, University of Arizona, Tucson, Arizona, USA.

³Department of Geological Sciences, Brown University, Providence, Rhode Island, USA.

⁴Ashima Research, Pasadena, California, USA.

Corresponding author: Michael A. Mischna, Jet Propulsion Laboratory, California Institute of Technology, Pasadena, CA 91109, 4800 Oak Grove Dr., M/S 183–601, Pasadena, CA 91109, USA. (michael.a.mischna@jpl.nasa.gov)

martian atmosphere. Interestingly, it was noted more than a decade ago in *Carr* [1996], “...current climate models cannot be satisfactorily reconciled with the concept of an early, warm and wet Mars.” Despite great advances in Mars climate modeling between then and now, this statement remains as true today as when written.

[4] In an attempt to address this seemingly intractable problem, other suggestions for the provenance of surficial fluvial features dated to the Noachian have been introduced, each of which attempts to explain how such morphology could be established in the absence of long-term warm conditions. *Squyres and Kasting* [1994] put forth the idea that hydrothermal convection beneath the surface is responsible for the production of liquid water at the surface and that such episodic and localized surface water could flow for tens to hundreds of kilometers before freezing, explaining the observed valley systems. *Segura et al.* [2002, 2008] have suggested that moderate-to-large-sized impactors (>30 km), which would have been more frequent during earlier periods of martian history, would have produced periodic warm and rainy conditions for the years to decades following impact and near-surface temperatures above 273 K for even longer—a process that can provide a source of liquid for the many observed features on the surface.

[5] Recently, a study by *Ehlmann et al.* [2011] suggested that the observed clay minerals at the martian surface could all have been formed through interactions with subsurface water and subsequently exposed through surface erosion, precluding the need for interaction with the near-surface hydrological cycle and the warm, wet conditions suggested by its presence. While a novel assertion, it does not appear to be able to explain the presence of all the clays observed at the surface. *Ehlmann et al.* [2011] used the detection of observed hydrated minerals to understand climate in the Noachian on Mars, but minerals serve as poor proxies for the local climatic conditions because it cannot be determined if they are detrital in nature and formed in the deep crust (consistent with the cold climate hypothesis) or authigenic and formed generally in place at the surface (which supports the warm, wet hypothesis). Without question, some of the clay minerals were formed in sedimentary rocks created at the surface, and therefore, they must have formed in wet (and, hence, warm) environments. A study by *Halevy et al.* [2011] of carbonate inclusions in the ALH84001 meteorite found that, based upon isotopic fractionation, the inclusions were formed at a surface temperature of $\sim 18^\circ\text{C}$ in a near-surface aqueous environment, pointing to a warm environment for at least some time. As one of the few direct data points of the early martian climate, it points strongly towards an environment that was somewhat clement, although the duration of such conditions cannot be precisely known.

[6] Apart from the alternative arguments presented above, the notion that early Mars had a warmer and wetter environment due to greenhouse warming by one or more gases remains, perhaps, the most widely explored means of explaining the observed surface geochemistry and geomorphology.

[7] The idea that sulfur-bearing gases may have contributed to an early greenhouse is an intriguing one that has been both periodically and recently revisited [*Postawko and Kuhn*, 1986; *Yung et al.*, 1997; *Halevy et al.*, 2007; *Johnson*

et al., 2008, 2009; *Tian et al.*, 2010]. The behavior of such species (specifically, SO_2 and H_2S) is sufficiently complex that there is little certainty as to the net effect of sulfur in the early martian atmosphere and the effect may be time varying. The presence of sulfur-bearing gases in the early martian atmosphere is expected; both sulfur dioxide and hydrogen sulfide are common products from volcanic outgassing on Earth and are similarly expected from outgassing and eruptive volcanic events on Mars. Indeed, sulfur-bearing minerals appear to be an important component of the geologic rock record on Mars and point to an active sulfur cycle [*McLennan and Grotzinger*, 2008; *King and McLennan*, 2010]. Both sulfur dioxide and hydrogen sulfide gas are absorbing in the infrared, identifying them as possible greenhouse candidates. Suggestions that sulfur dioxide (SO_2) in particular may have acted as an effective greenhouse warmer have been around for some time. Early results from *Postawko and Kuhn* [1986] with a 1-D, annually averaged model indicated that levels of 1000 ppm could contribute to as much as 8–10 K of warming, although, as a 1-D model, that study was limited to globally averaged conditions and did not generally explore the possibility of localized niches becoming warmer or exceeding the 273 K threshold for liquid water.

[8] More recently, *Johnson et al.* [2008] performed a modeling investigation of the warming influence of volcanically introduced SO_2 into the early martian atmosphere using a 3-D GCM. For background atmospheres of both 50 mb and 500 mb CO_2 , and in the presence of water vapor, the role of SO_2 as an additional greenhouse gas was explored. Unlike prior investigations, these results showed a potentially significant feedback cycle between water vapor and SO_2 (although the feedback was not strictly limited to SO_2). Specifically, the warming contribution of SO_2 was thought to act as a “trigger” in the climate system, raising the mean global surface temperature enough such that significantly greater abundances of water vapor could enter the atmosphere, with the water vapor ultimately acting as the dominant greenhouse gas. These results were surprising and did not agree with the prior investigations, leading to a potential avenue by which early Mars could have sustained warmer temperatures.

[9] Here, we re-evaluate, in part, the work in *Johnson et al.* [2008] using an improved version of the radiation code used in that study along with a consideration of relevant orbital parameters. The improvements to the radiation code are based on more recent suggestions of appropriate line shape parameters and collision-induced absorption and continuum functions than were used previously [*Halevy et al.*, 2009; *Wordsworth et al.*, 2010]. We use a correlated- k approach [*Mischna et al.*, 2012] to solve the equations of radiative transfer for multiple-gas atmospheres ($\text{CO}_2 + \text{H}_2\text{O} + \text{SO}_2$) using the same atmospheric conditions studied in *Johnson et al.* [2008].

[10] In section 2, we provide a brief discussion of the evidence for warm conditions during early Mars history. In section 3, we discuss the underlying concept of a trace gas/obliquity-regulated greenhouse cycle. A description of both the climate model and radiation algorithms is presented in section 4, and section 5 presents results from our model for a range of conditions possible on early Mars. We interpret these results in section 6.

2. Background

[11] While they may seem, *prima facie*, wholly independent, greenhouse warming and obliquity have a closely linked role in regulating climate through martian history. While at present, the climate is modified predominantly by changes in obliquity with a minimal role for volcanism and greenhouse warming, during the Noachian, especially during the development of the Tharsis rise, the reverse was likely true, and obliquity oscillations played a secondary role within a volcanically dominated martian climate. The transitional period between these two end-member conditions was extensive, and findings of post-Noachian fluvial formations on the surface [Mangold *et al.*, 2004, 2008] point to a Hesperian climate where obliquity may have played a significant role in regulating the climate by serving as the “switch” that transitioned Mars between cold/dry and warm/wet periods.

2.1. Geologic Evidence for Warm Conditions Through Martian History

[12] The role of water during the early periods of martian history was likely substantial. There is widespread evidence of aqueous alteration of hydrous minerals present in terrains that date to the Noachian period (4.5 to 3.7 Ga). Results from OMEGA (*Observatoire pour la Mineralogie, l'Eau, les Glaces et l'Activité*) on board Mars Express reveal the widespread presence of phyllosilicate minerals [Poulet *et al.*, 2005; Bibring *et al.*, 2006] mapped to the oldest, Noachian-aged surfaces. More recent results from Carter *et al.* [2010] have identified ancient hydrated silicates in crustal outcrops of the martian northern plains. These hydrous materials, which may represent aqueous alteration of igneous rocks or direct precipitation out of fluids, point to a global warm and wet Noachian period on Mars. Following the Late Heavy Bombardment (~3.8 Ga), it is generally believed that there was a gradual cooling of the surface environment, due to decreased internal heat flux and a steady erosion of the atmosphere, such that by ~3.5 Ga the character of the surface environment had changed substantially. Whereas many Noachian-aged surfaces contain phyllosilicate (clay) mineral assemblages, whose formation requires the presence of water, there are fewer terrains of Hesperian age that show the clear signature of enduring water. Discovery of Hesperian-aged hydrated silicates such as opal in regions adjacent to Valles Marineris [Milliken *et al.*, 2008] do require the presence of water to form; however, the low abundance of quartz on the surface along with enhanced levels of opal-A and opal-CT indicates that the conversion to quartz was incomplete, and, hence, the duration of water interaction at the surface was limited after the opal was formed [Tosca and Knoll, 2009]. Regional valley networks [Mangold *et al.*, 2004, 2008] that cut through Hesperian-aged terrain adjacent to Echus and Melas Chasmata also suggest precipitation during the Late Hesperian, and thus warmer conditions at least periodically during this period. The presence of these younger fluvial features on the surface indicates at least the temporary presence of liquid water at the surface on either a regional or global scale.

2.2. Post-Noachian Fluvial Activity: Competing Hypotheses

[13] Multiple hypotheses [e.g., Clifford and Parker, 2001; Baker, 2009] present differing scenarios of how the climate

may have evolved during this period of martian history (Figure 1); there are two leading explanations for the formation of fluvial surface features in the post-Noachian terrains. The first argues that a secular decrease in internal heating produced a martian climate that was largely cold and dry by the time of the Noachian-Hesperian transition. Fluvial surface features dated to the post-Noachian are explained as being a response to local enhancements in hydrothermal circulation or subsurface heat flow [Squyres and Kasting, 1994; Gulick, 2001]. In other words, these features are a response to *local*, rather than *global*, climate change. The near-surface environment has responded to this decrease in internal heating by the gradual thickening of the cryosphere over time [Clifford and Parker, 2001], reducing the likelihood of water at the surface. This theory can be visualized in terms of the relative “ease” of supporting surface liquid by the “Secular Decrease” curve in Figure 1.

[14] The second theory was originally conceived by Baker *et al.* [1991] and is known by the moniker Mars Episodic Glacial Atmospheric Oceanic Upwelling by Thermotectonic FLood Outburst (“MEGAOUTFLO”). The MEGAOUTFLO theory argues for episodic enhancements in heat flow and volcanism, which result in short-duration periods throughout martian history that are *globally* warmer and wetter than those at present (Baker [2009]; Figure 1, “MEGAOUTFLO” curve). The presence of post-Noachian fluvial erosion in the highland valleys [Baker and Partridge, 1986; Bradley *et al.*, 2002], valley networks on Alba Patera [Baker *et al.*, 1991] and adjacent to Valles Marineris [Mangold *et al.*, 2004], young fluvial formations in Medusa Fossae [Bradley *et al.*, 2002] and many apparently warm-based glacial features [Baker, 2001] are all seen as consistent with these periodic warming episodes in the martian climate during the post-Noachian period. Mars Express High-Resolution Stereo Camera observations of Mars have bolstered this idea of episodic volcanic activity spanning most of post-Noachian martian history [Neukum *et al.*, 2004; Werner, 2009]. In MEGAOUTFLO, thermal and/or tectonic effects associated with large mantle plumes result in the release of large amounts of radiatively active gases (in the original MEGAOUTFLO concept, these gases are primarily CO₂ and CH₄), which produce massive, explosive outbursts of water and sediment, flooding the martian Northern Plains with a large-scale northern ocean and initiating a widespread greenhouse effect across the planet from the once-subsurface reservoirs of CO₂, H₂O and other trace gases. These periodic outbursts are short-lived (10³-10⁵ years) and the age of the observed landforms seems to suggest that these episodes were longer in duration during the Noachian, and have grown progressively shorter with time.

3. Trace Gas/Obliguity Interaction

[15] As discussed in section 1, there have been no completely satisfactory explanations for how a greenhouse atmosphere, alone, could have maintained a wet early Mars in light of the reduced solar luminosity [Gough, 1981; Sackmann and Boothroyd, 2003] expected during the Noachian. One investigation using a GCM to study an early Mars environment with moderate CO₂ atmospheres and high levels of atmospheric SO₂ [Johnson *et al.*, 2008] produced an interesting result. Confirming previous investigations [e.g., Postawko and Kuhn, 1986], the individual greenhouse roles of H₂O and SO₂ were

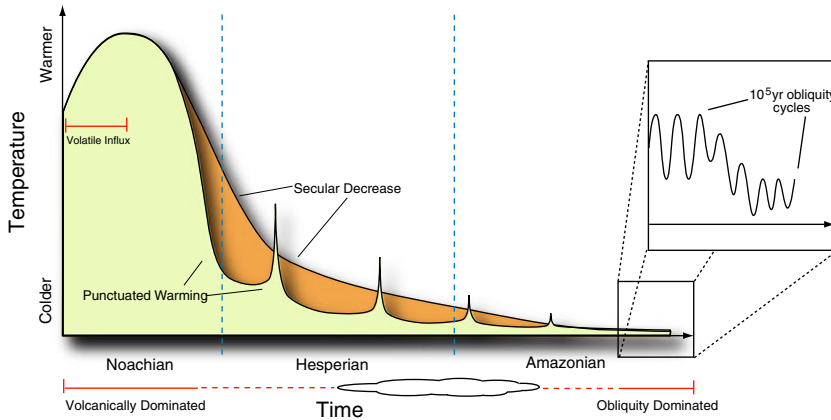


Figure 1. Two possible timelines for the level of aqueous activity at the martian surface: a steady, secular decrease with time having little aqueous activity since the Late Hesperian or the MEGAOUTFLO scenario with generally low, but episodically high, water activity throughout history. Both scenarios envision a warm, wet, volcanically dominated Noachian beginning with the early influx of volatiles from planetary bombardment and are consistent with a present-day obliquity-dominated climate. Changes in aqueous activity today are controlled by shifts in axial tilt over the 10^5 year obliquity cycle (enlarge).

found to be small at low martian temperatures, even in a background atmosphere of tens to hundreds of millibars of CO_2 . However, the volcanic emission of certain greenhouse gases, while themselves not sufficient to provide the warming required for surface liquid, appeared to have acted as a “trigger” to elevate the mean atmospheric temperature to a point at which water vapor became the dominant greenhouse gas, and could have remained so for some time following photochemical loss or rainout of the initial volcanic species.

[16] Conditions expected during the Late Noachian-Early Hesperian period provide such an avenue by which high levels of water vapor can be sustained for not-insignificant periods of time. The initial rise in temperature from the volcanic outgassing imparts the needed warming to spur greater influx of water vapor into the atmosphere from extant surface and near-surface reservoirs. Paleoclimate photochemical modeling by Johnson *et al.* [2009] estimates the lifetime of the large amounts of SO_2 in the early martian atmosphere, from Johnson *et al.* [2008], to be 10^3 - 10^4 years, providing an extended period under which large-scale surface water reservoirs can develop. For lesser SO_2 abundances, the atmospheric lifetime would be correspondingly shorter, but the actual abundance that could be reached during an individual outgassing episode still remains an open question and was, presumably, episodically variable. So long as the atmosphere is in contact with this surface water, the atmosphere will remain humid. (Liquid water is not strictly necessary, but its presence implies higher atmospheric temperatures and thus a larger water vapor capacity). Following the eventual loss of the volcanic trace gases, atmospheric temperatures will return to their pre-“trigger” values, buffered somewhat by the transient presence of any surface water as the overall system slowly cools.

[17] Conventional wisdom argues that a species like SO_2 (and H_2S , through its oxidation) would make a poor greenhouse gas because of its high solubility and participation in photochemical pathways that lead to sulfate aerosols. Such aerosols have a penchant for scattering incoming sunlight and thus are thought to act as a net cooling mechanism

[e.g., Tian *et al.*, 2010]. The photochemical modeling of Johnson *et al.* [2009] indicates, however, that this might not be the case in an ancient martian atmosphere that was more reduced than today. The chemical pathway from SO_2 to SO_4 aerosols requires radical species (primarily OH^-) in order to proceed. Under the thicker (and more reducing) ancient martian conditions, these radical species would be highly depleted below the ancient martian tropopause. Therefore, even though SO_2 would have been abundant, there would be too few available oxidants for efficient conversion of SO_2 into sulfate, and thus minimal scattering (and cooling) of the atmosphere. Further, loss of SO_2 dissolved in rainwater would be limited by surface water saturated in SO_2 [Johnson *et al.*, 2009].

[18] In contrast, Tian *et al.* [2010], using an approach that considered the radiative effects of sulfate aerosols, argued that the transient warming period should be on the order of months, not years (nor centuries), due to the eventual cooling effect introduced by scattering from airborne sulfate aerosols. Both approaches concede that numerous volcanic events (up to $\sim 10^4$) are consistent with best estimates of total maximum sulfur outgassing from the formation of the Tharsis province [Halevy *et al.*, 2007].

[19] Today, martian climate is largely controlled by the planet’s obliquity, or axial tilt. While presently at a moderate 25° , the obliquity of Mars oscillates with a period of $\sim 10^5$ years and, within the past 20 Myr, has ranged between 15° and 45° [Laskar *et al.*, 2004]. There is substantial evidence that these shifts in obliquity are the key drivers of recent martian climate. GCM modeling of Haberle *et al.* [2003], Mischna *et al.* [2003] and Forget *et al.* [2006] find that under periods of higher obliquity ($>\sim 35^\circ$), polar surface ice is mobilized and transported to lower latitudes, where it is thermodynamically stable. These studies confirm the early predictions of Jakosky and Carr [1985]. At obliquities of 45° and higher, ice is stable at the equator. Geomorphological evidence of mid-latitude glacial deposits [Christensen, 2003; Milliken *et al.*, 2003; Head *et al.*, 2005; Plaut *et al.*, 2009], mantled and desiccated terrain [Mustard *et al.*, 2001;

Head et al., 2003], and the regularity of polar layered deposit sequences [Milkovich and Head, 2005; Limaye et al., 2012] strongly point to control of surface volatiles by this 10^5 year cycle.

[20] It is not unreasonable, then, to assume that obliquity played a role in modifying martian climate from the outset. Today, in the presence of a thin CO_2 atmosphere and with no widespread volcanism, the amount of water vapor in the atmosphere is relatively small, even at high obliquities, and this has likely helped to sustain the cold/dry climate during the Amazonian. During the more geologically active Noachian, however, volcanism was more widespread and there were stronger contributions from greenhouse gases in the thicker atmosphere.

[21] Through its control on the amount of atmospheric water vapor, the obliquity cycle acts as a natural regulator for the strength of the water vapor greenhouse on Mars. The regular oscillations in Mars' axial tilt bring the planet into and out of periods of alternating wetter and drier conditions. Under the present-day obliquity (and under present atmospheric conditions), the atmosphere is dry, and the availability of moisture is controlled by the temperature of water ice exposed in the northern polar cap. During periods of higher obliquity, the annual average polar temperatures also rise, increasing the level of water vapor released into the atmosphere [Jakosky and Carr, 1985; Mischna et al., 2003; Mischna and Richardson, 2005]. Jakosky and Carr [1985] suggest water vapor levels over the poles \sim 50–100 times greater than the present-day value for an obliquity of 45° . While peak levels may be somewhat overestimated based on the development of sediment lag deposits over time [Mischna and Richardson, 2005], there will still be a greater abundance of water in the atmosphere at higher obliquities. Conversely, as the obliquity decreases to zero, the poles act as cold traps, which efficiently removes water vapor from the atmosphere. However, regardless of the obliquity and amount of atmospheric water vapor, the current martian climate system remains too cold to sustain liquid water at the surface.

[22] The same cannot be said for earlier epochs when a somewhat thicker CO_2 atmosphere and more vigorous volcanic activity elevated atmospheric temperatures to the point that these oscillations in obliquity may have had a real and significant control on whether the system fell above or below the nominal freezing point. Conceptually, the control of obliquity on temperature is illustrated in Figure 2. In the absence of widespread volcanic emissions, such as today, the mean global surface temperature (red, dashed curves) varies only slightly over obliquity cycles, and it remains at least several tens of degrees below the nominal freezing point (a portion of an identical, "nominal" obliquity cycle is illustrated at the top for each of the three martian epochs.) During periods of increasing or sustained high obliquity, higher water vapor levels are supported in the atmosphere. If, during this high obliquity period, there is an event that elevates volcanic trace gas levels, even more water vapor can enter the atmosphere, raising temperatures (lower solid black curves) above the freezing point. This effect is negligible in the cold/dry Amazonian climate, and therefore sustained liquid water is not possible. During the Noachian, prolonged volcanism (and a thicker CO_2 atmosphere) would have overwhelmed the modifying effects of obliquity,

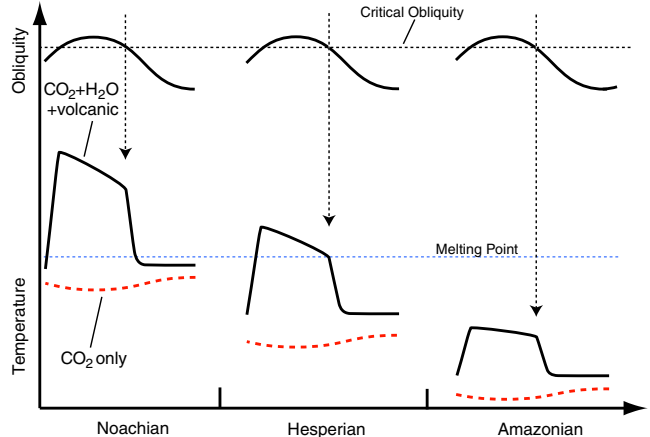


Figure 2. The role of the water vapor feedback effect in each of the three martian epochs for a similar obliquity cycle. In the Noachian, CO_2 -only temperatures (red line) are near the melting point and change minimally over the cycle. Introduction of volcanic gases "activates" the water vapor feedback, sustaining warm temperatures until obliquity falls below some "critical" value. In the Hesperian, periodic volcanism similarly raises temperatures but may be more strongly limited by the obliquity phase. The presence of surface water sustains higher vapor levels (and consequent warming) for some time after loss of volcanic gas. This feedback is maximized at high obliquity (allowing liquid water) and squelched as obliquity drops. In the Amazonian, temperatures remain below the melting point, regardless of obliquity, and stable liquid is not possible.

allowing the presence of liquid water by this method almost regardless of tilt. It is during the Hesperian that surface temperatures are most dramatically influenced by shifts in obliquity. Once high, temperatures above the melting point of water ice can be temporarily sustained so long as obliquity remains high and surface water is available to humidify the atmosphere. As obliquity begins to decrease and surface reservoirs freeze, water vapor levels fall and the entire system "crashes" back to a cold, dry state.

[23] Our avenue for exploring this proposed idea involves the use of a 3-D GCM that is capable of modeling the climate conditions believed to be present during early martian history. By setting the most influential orbital parameters and adjusting the amount of water vapor present in the atmosphere, we can examine the range of conditions that are plausible in the early martian climate both during and after one of these large volcanic events and on the timescales of the orbital cycles.

4. Model Description

4.1. MarsWRF General Circulation Model

[24] Atmospheric circulation on Mars is simulated using the Mars Weather Research and Forecasting (MarsWRF) GCM. MarsWRF is a global model derived from the terrestrial mesoscale WRF model [Michalakes et al., 2004; Skamarock et al., 2005; Skamarock and Klemp, 2008] and is a Mars-specific implementation of the PlanetWRF GCM [Richardson et al., 2007]. MarsWRF solves the primitive equations using a finite difference model on an Arakawa C

grid. The horizontal resolution of the model is variable and selectable at runtime, and the vertical grid follows a modified-sigma (terrain-following) coordinate with resolution also selectable at runtime. For validation purposes, the total present-day atmospheric CO₂ budget has been tuned [Guo *et al.*, 2009] to fit the Viking Lander annual pressure curves (~ 6.1 mb) before the pressure is scaled upwards to reflect the thicker early martian atmosphere. Surface albedo and thermal inertia are matched to MGS-TES observations [Christensen *et al.*, 2001; Putzig *et al.*, 2005] except where noted for specific investigations. Water ice albedo and emissivity are fixed at 0.45 and 1.0, respectively, while corresponding values for CO₂ ice are independently chosen for each hemisphere [Guo *et al.*, 2009], although this does not appreciably affect our results. Under these thicker-atmosphere conditions, we do not impose a permanent south polar CO₂ ice cap but replace it with a permanent H₂O ice cap of similar size. We use a model resolution of $5^\circ \times 5^\circ \times 40$ vertical layers, (from 0–80 km). Orbital and axial parameters are readily adjusted in MarsWRF, which makes it straightforward to examine Mars at conditions of varying obliquity. At different obliquities, surface albedo and thermal inertia maps are modified in response to the deposition of ice on the surface at each location. This process follows from Mischna *et al.* [2003]. A basic water cycle is present in MarsWRF, allowing for the formation of water ice clouds (although they are not radiatively active here), including particle sedimentation and transport.

4.2. KDM Radiation Code

[25] We have developed a multigas, two-stream radiation referred to as the KDM model [Mischna *et al.*, 2012] loosely based on the structure outlined in Edwards and Slingo [1996] but modified to use the *k*-distribution radiative transfer method. This method retains much of the accuracy of line-by-line calculations but is significantly faster, making it ideal for computationally expensive 3-D global models. Details about the correlated-*k* method are widely found in the literature [e.g., Lacis and Oinas, 1991; Fu and Liou, 1992], and information about the particular implementation used here may be found in Mischna *et al.* [2012]. We provide only a brief description of the approach here.

[26] Conceptually, the “trick” to the correlated-*k* method involves partitioning the solar/IR spectrum into distinct spectral bands and resorting the absorption curve within each band (which is highly variable as a function of wavelength) to produce a smooth curve of line strength that is more conducive to numerical approximation. In the present implementation, the full solar/IR spectrum is partitioned into 14 bands (seven solar, seven IR, from 0.24 to 1000 μm) of varying widths. The absorptivities within each band are then sorted by strength. This sorted curve no longer maps line intensity directly to wavelength but instead maps intensity to the cumulative probability function, i.e., “What fraction of the intensities are smaller than the given intensity?” Atmospheric transmissivity, Tr , is calculated by numerical integration of this smooth curve using a 32-point double Gaussian quadrature (split at 0.95) according to

$$Tr = \sum_{i=1}^{32} a_i \exp[-k_i u]$$

where k_i are the absorption coefficients at each of the 32 quadrature points, a_i are the corresponding weights obtained from the Gaussian quadrature (which are fixed across all spectral bands and all atmospheric conditions), and u is the mass of the absorbing gas in the optical path (ku is more commonly known as τ —atmospheric opacity).

[27] Absorption coefficients are stored offline in a LUT. Coefficients are stored from 50 to 400 K with 20 K spacing and from 10^{-4} to 10^6 Pa with $\log(p)=0.4$ spacing. Water vapor is allowed to vary in the climate model, and gas mixtures with variable water vapor amounts from 10^{-7} to 10^{-1} (by decade) along with a water-free mixture are stored in the LUT. We assume a fixed amount of SO₂ present in the atmosphere, a 2.45×10^{-4} mixing ratio, mimicking the high limit used in Johnson *et al.* [2008] for a 500 mb atmosphere, based on estimate of Wilson and Head [2002]. Our choice here is designed to provide the best-case scenario for achieving warm conditions. Lesser amounts of SO₂, such as the lower limit used in Johnson *et al.* [2008] (still a significant concentration requiring a high level of volcanic outgassing), will produce less warming. In this sense, if warm temperatures cannot be achieved in our present model, then they likely cannot be achieved with lesser SO₂ abundances.

[28] The radiation code has been incorporated into the MarsWRF general circulation model and the GCM is run forward for two martian years with output every 3 hours. Results are analyzed for the second Mars year. Simulations (not shown) of surface temperatures have been run out for as much as seven Mars years and show no appreciable differences beyond the second year. Solar luminosity has been reduced to 75% of the present-day value to reproduce the faint young Sun experienced in early martian history, and dust is excluded from the atmosphere as the abundance and distribution of dust is unknown in the early Mars environment.

5. Model Runs

5.1. Present Obliquity (25°)

[29] Our choice of SO₂ mixing ratio is based on the maximum estimated abundance from Johnson *et al.* [2008] for a 500 mb baseline CO₂ atmosphere (245 ppm), which yielded the maximum level of warming among their scenarios. By choosing atmospheric conditions that maximize greenhouse warming, we can provide an upper limit on not only the global average temperatures that may be obtained but also localized variations that may provide isolated regions of enhanced warming.

5.1.1. Baseline

[30] For the baseline simulation, we have run the MarsWRF GCM with an atmosphere of 500 mb CO₂ and no other radiatively active atmospheric gases. Annually averaged surface temperatures for the last year of the simulation are shown in Figure 3a. Peak annually averaged equatorial temperatures reach ~ 235 K, with a globally averaged value of 219 K (Table 1). This is within a couple degrees of the value obtained by Johnson *et al.* [2008] and not too dissimilar from the current average surface temperature. The increased greenhouse potential of the thicker CO₂ atmosphere is offset by the reduction in solar luminosity.

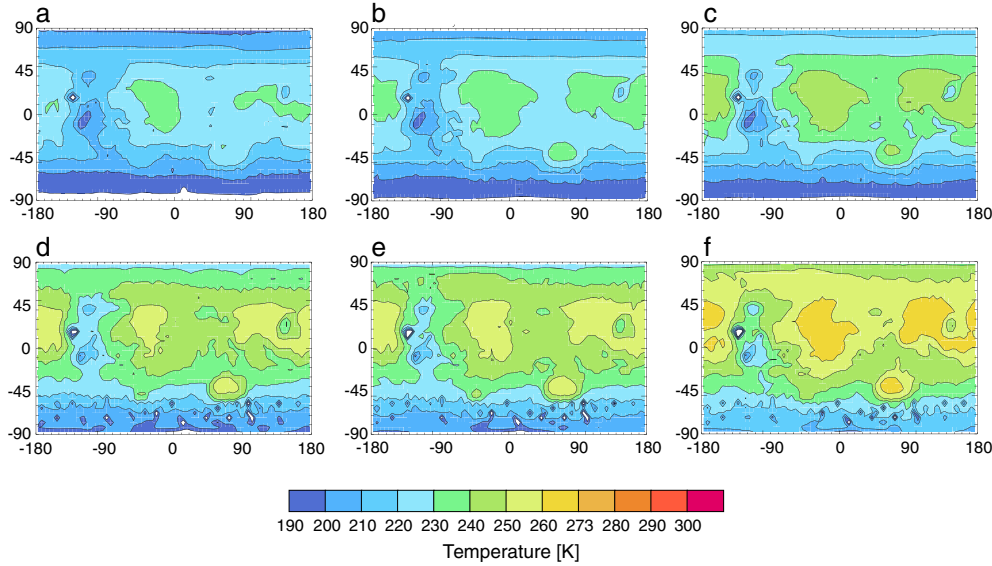


Figure 3. Mean annual surface temperatures for a 500 mb CO₂ atmosphere for the various simulations run in this investigation. (a) CO₂-only atmosphere, (b) with standard water cycle, (c) with saturated atmosphere, (d) with SO₂, (e) with SO₂ and standard water cycle, and (f) with SO₂ and saturated atmosphere.

Table 1. List of Simulations Run in This Study and Their Relevant Parameters

Atmospheric Gases	Obliquity (Albedo)	Saturated Atmosphere?	Global/Annual Mean Surface Temperature ^a	Peak Annual Surface Temperature ^b
CO ₂	25	N	218.6	235.4
CO ₂ + H ₂ O	25	N	221.9	239.1
CO ₂ + H ₂ O	25	Y	228.8	250.1
CO ₂ + SO ₂	25	N	236.6	258.2
CO ₂ + SO ₂ + H ₂ O	25	N	238.7	259.9
CO ₂ + SO ₂ + H ₂ O	25	Y	246.9	267.6
CO ₂ + SO ₂ + H ₂ O	5	N	241.9	265.2
CO ₂ + SO ₂ + H ₂ O	15	N	240.5	263.5
CO ₂ + SO ₂ + H ₂ O	45	N	234.1	253.6
CO ₂ + SO ₂ + H ₂ O	60	N	231.4	248.8
CO ₂ + SO ₂ + H ₂ O	15	Y	249.0	271.2
CO ₂ + SO ₂ + H ₂ O	45	Y	244.5	262.1
CO ₂ + SO ₂ + H ₂ O	60	Y	243.2	259.8
Northern Hemisphere Surface Tests ^c				
CO ₂ + SO ₂ + H ₂ O	25 (0.12)	N	248.0	277.1
CO ₂ + SO ₂ + H ₂ O	25 (0.08)	N	249.3	278.9
CO ₂ + SO ₂ + H ₂ O	25 (0.08)	Y	267.0	292.5

^aAverage temperature value across entire Mars year over the entire surface.

^bMaximum annually averaged temperature anywhere on the surface.

^cTemperature values reflect stated conditions in the northern hemisphere only.

[31] Perhaps more significant for understanding the likelihood of sustaining liquid water at the surface is a measure of the fraction of the year for which surface temperatures are at or exceed a nominal melting temperature. As a conservative assumption, we use 273 K for pure water, although melting temperatures for brine solutions may be many tens of degrees lower than this [Clark and Van Hart, 1981; Hecht *et al.*, 2009]. Figure 4a illustrates the percentage of the year for which surface temperatures exceed 273 K in the baseline simulation. In our CO₂ only case, only rarified locations will ever see conditions above melting, generally restricted to the southern mid-latitudes and even then for <10% of the martian year (on the order of 50–60 sols). This does not suggest temperatures over 273 K for continuous periods but rather 50–60 days where noontime peak temperatures may exceed 273 K for perhaps an hour or two. This is

highlighted in Figure 5a, which shows the longest duration within the year for which temperatures remain consistently above 273 K. As expected, no surface location exceeds this threshold continuously for more than a few hours. The distribution of these locations in the south reflects the influence of the spin axis orientation, which, in these simulations, mimics the present-day condition, where southern summer coincides with perihelion and thus, summertime temperatures are warmer in the south than the north. Reversing this orientation puts warmer temperatures in the northern hemisphere.

5.1.2. Water Vapor

[32] Water vapor may have a potentially significant greenhouse impact in the atmosphere. The magnitude of this effect is explored by considering two separate scenarios. In the first, we examine the magnitude of warming achieved by introducing a nominal atmospheric water cycle into the

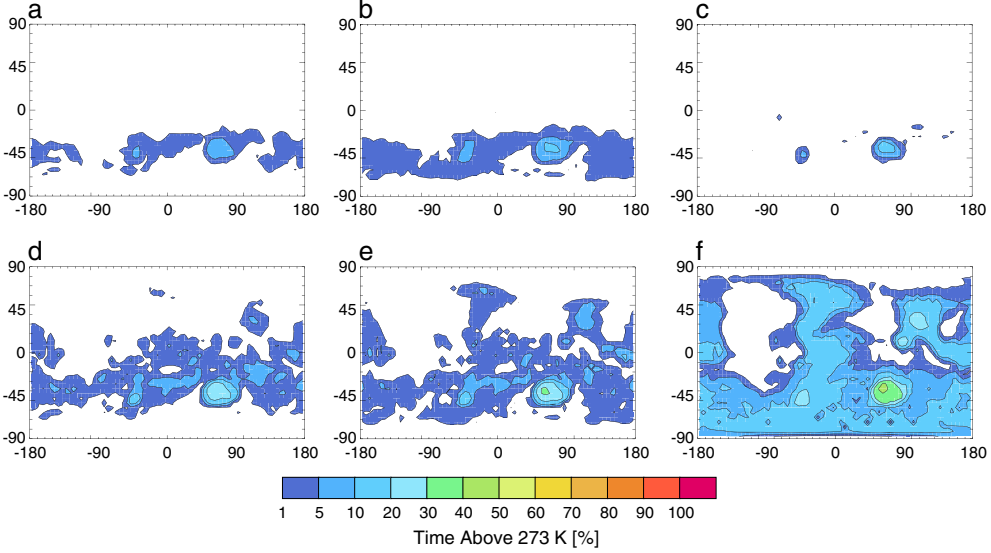


Figure 4. Fraction of the year for which surface temperatures exceed 273 K for the same simulations as in Figure 3. Areas in white experience such temperatures <1% of the martian year.

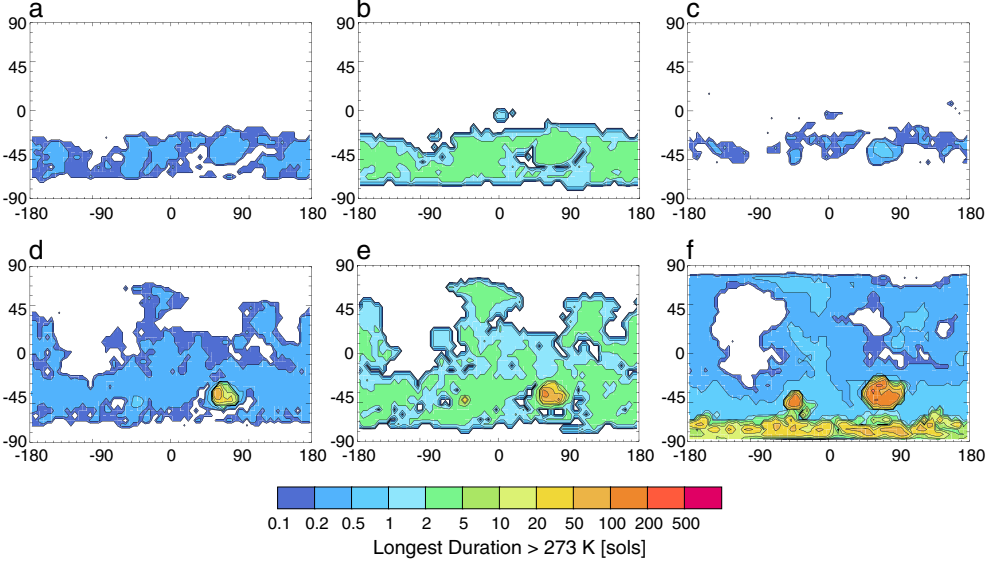


Figure 5. Longest duration (in sols) over which temperatures continuously exceed 273 K for the same simulations as in Figure 3. Areas in white experience such temperatures at no point during the martian year.

martian system. This simple cycle allows water vapor to sublime off polar caps (present in both hemispheres) and into the atmosphere. Where saturated, water ice can form in the atmosphere and fall to the surface. We do not include the radiative effect of water ice clouds in this situation as we are considering gas phase warming only. Figure 6 illustrates the column-integrated annual water vapor abundance for this simple water cycle model (referred to as the “standard” Mars water cycle).

[33] Net warming over the CO₂-only atmosphere is shown in Figure 7a and reveals only nominal warming planet-wide, with slightly higher warming of about 5–6 K in the north polar regions adjacent to the large residual polar cap. Water vapor is being sublimed off the residual polar caps during their respective summers, which manifests itself as seasonal maxima at these latitudes during the summer seasons. This

behavior is not unlike present-day Mars but without the presence of a residual CO₂ ice cap in the south, which inhibits water vapor sublimation during southern summer.

[34] To determine the upper limit of warming from water vapor, the second scenario prescribes a time-dependent and location-dependent mixing ratio at each model grid point equal to the local saturation vapor pressure (determined by the local temperature). Again, cloud formation is ignored, although more likely to occur under these (contrived) conditions than in our standard Mars water cycle scenario. Such a saturated atmosphere provides substantially more warming to the early Mars climate than the standard water cycle, with increases of ~20 K found in the northern polar regions (Figure 7b). The warming distribution generally follows the topography and overall atmospheric column depth.

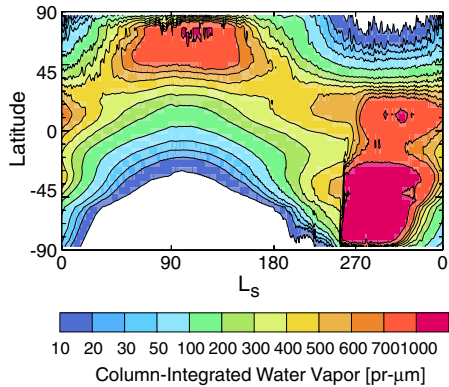


Figure 6. Column-integrated water vapor profile ($\text{pr } \mu\text{m}$) for the standard water cycle. Both poles have exposed water ice caps, resulting in a greater influx of water from the south compared to the present-day situation.

[35] For both of these scenarios, the presence of water vapor does not significantly increase the likelihood of surface liquid water—the longest duration of temperatures consistently above 273 K increases to 1–2 sols during the peak summer months (Figures 5b and 5c), which may allow for localized flow of water were, for example, a surface source to be present. Interestingly, for the saturated atmosphere, it appears that the likelihood slightly decreases over both the CO_2 -only and standard water cycle scenarios. We interpret this behavior as being the effect of high levels of water vapor in the warm lower atmosphere actually reducing the amount of shortwave radiation reaching the surface, with this shortfall being taken up in the atmosphere itself.

[36] This peculiar behavior is illustrated in Figure 8, which, in the left panel, shows the zonally averaged downward shortwave (solar) flux at the surface for both the “standard” water cycle case (solid line) and the saturated atmosphere case (dashed line) around southern summer solstice. The reduction in surface flux in the saturated

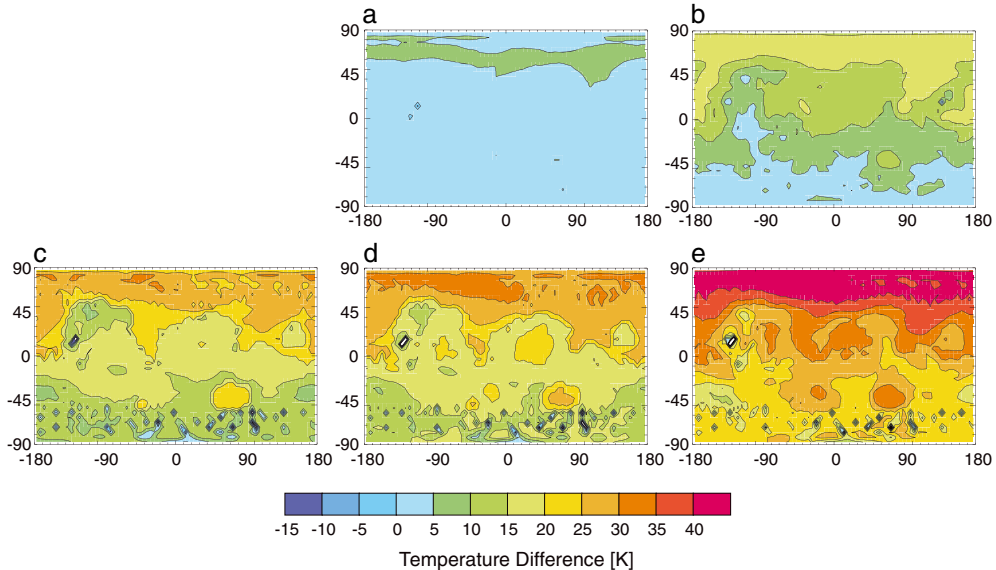


Figure 7. Level of greenhouse warming (in K) for the same simulations as in Figure 3 relative to a 500 mb CO_2 atmosphere (Figure 3a). The “missing” panel reflects lack of temperature differences when comparing Figure 3a to itself.

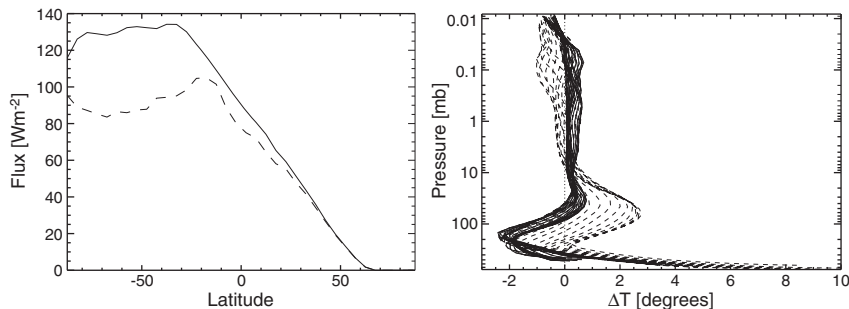


Figure 8. (Left) Zonally averaged downward visible solar flux (in W m^{-2}) at a single time at southern summer solstice for the “standard” water cycle (solid) and saturated water cycle (dashed) cases. (Right) Zonally averaged temperature difference (in K) between the “standard” and saturated cases for the same time period. Positive values mean saturated case is warmer than “standard” case at that altitude. Solid lines indicate profiles in the southern hemisphere and dashed lines for the northern hemisphere.

atmosphere is evident in the southern hemisphere where temperatures are warmest and water vapor content of the saturated atmosphere is greatest. The zonally averaged temperature difference (ΔT) in each of the 36 model latitude bands between the two simulations during the same time period is shown in the right panel of Figure 8. The solid lines, corresponding to latitudes in the southern hemisphere, show a distinct pattern, with slightly positive values above ~ 50 mb (positive indicates the saturated case is warmer) and mostly negative values below, including at the surface, which is reflected in the results of Figures 7b and 7c, for which the likelihood of surface liquid water is slightly greater for the drier “standard” water cycle. At pressures above ~ 200 mb, the trend in ΔT reverses, and values tend towards the positive; however, the higher elevation of the southern hemisphere (having, hence, lower surface pressures) prevents the saturated case from again being warmer at the surface. A similar overall behavior is observed in the northern (wintertime) hemisphere, which is represented by the dashed lines, but the effect of the lower topography can be seen by the more strongly positive temperature differences at the surface. As the north is the winter hemisphere in this case, we would not expect either scenario to yield temperatures > 273 K during this season, which is consistent with Figure 7a or 7b.

5.1.3. Sulfur Dioxide

[37] Next, we explore the magnitude of the greenhouse contribution from SO_2 alone by adding SO_2 into the model atmosphere and excluding water vapor. Figure 7c illustrates the warming contribution of SO_2 , which is more significant than that of water vapor. Peak temperatures in this simulation may be as much as 35 K warmer than CO_2 only, in line with, but greater than, the ~ 27 K warming seen in *Johnson et al.* [2008, Figure 4d]. As with water vapor, the pattern of warming generally mimics the surface topography, indicating that SO_2 is not optically thick at these abundances. There is a slight growth in the area for which surface temperatures exceed 273 K but not significantly greater than our previous cases.

[38] Despite the northern hemisphere experiencing the greatest relative warming, it remains the southern hemisphere that is, overall, the warmest. The deep Hellas basin has become a clear region of warm temperatures—above 273 K for $\sim 20\%$ of the year, all of which occurs contiguously during the southern summer, with localized subregions of Hellas maintaining warm temperatures for up to 100 consecutive sols.

[39] In Figures 7d and 7e, we reintroduce water vapor into the atmosphere using the standard water cycle and a saturated atmosphere, respectively. In the latter case, warming of > 40 K is found throughout the northern hemisphere high latitudes and warming of > 20 K globally. For these conditions, we begin to see conditions more conducive to the presence of liquid water. Much of the planet experiences conditions > 273 K for 10% of the year (Figures 4e and 4f), with the Hellas basin exhibiting such temperatures for nearly half of the year. With the exception of the Tharsis region, warm temperatures are achieved globally for at least a portion of the year.

[40] These results, however, are counter to the spectacular warming found by *Johnson et al.* [2008] which showed a maximum ΔT of ~ 70 K for the $\text{CO}_2 + \text{SO}_2 + \text{H}_2\text{O}$ simulation and nearly ubiquitous conditions above 273 K. The present radiation model is a significant improvement over the one used in *Johnson et al.* [2008] and incorporates several modifications that better capture the nature of the radiative

transfer, including incorporation of collision-induced absorption and continuum effects, a finer discretization of the spectral grid and better characterization of the 15 μm CO_2 band.

[41] *Mischna et al.* [2012] performed a rigorous validation of the present KDM scheme and found it to provide results consistent with line-by-line spectral models for both present-day and early Mars atmospheres. A reanalysis of the absorption model used in *Johnson et al.* [2008] shows similar results for present-day conditions but somewhat significant departures (relative to line-by-line models) for conditions of thicker and wetter atmospheres, resulting in an excess of atmospheric absorption and excessive surface temperatures. We are confident that the results presented here are superior to those in *Johnson et al.* [2008] and conclude that the results from *Johnson et al.* [2008], which were not adequately validated, incorrectly overestimated the amount of warming expected under these wet, thick atmosphere conditions, as they are noticeably distinct from both recent results and other, earlier work.

5.2. Obliquity Cycle

[42] In the previous section, we have seen that even under the most optimistic cases, at present-day obliquity and with a 500 mb atmosphere of CO_2 , H_2O , and SO_2 , it is difficult to sustain warm temperatures at the martian surface except for limited niches. The situation is further compounded by the orbital configuration of the planet. Under varying orbital conditions, the distribution of insolation varies markedly, which modifies the surface temperature distribution and hence the local saturation vapor pressure, which will impact the peak warming one can expect at the surface.

[43] Martian obliquity has a periodic cycle of $\sim 124,000$ years and oscillates regularly, with swings of as much as 30–40° per cycle. Numerical integrations have calculated martian obliquity back as far as 20 Myr [*Laskar et al.*, 2004] and have provided probability functions of martian obliquity (which is chaotic on longer timescales) throughout its history. At higher obliquity, during the summer months, the high latitudes are bathed in perpetual sunlight and achieve higher peak surface temperatures than at lower obliquities. Under these circumstances, the tropical regions of the planet serve as the atmospheric “cold trap,” with the corresponding migration of surface ice from the poles to the more stable equatorial region [*Mischna et al.*, 2003]. As we have seen in the previous section, it is the high northern latitudes that generally receive the greatest differential warming at present obliquity. It is worth investigating, then, what additional effect to localized warming may be contributed by a shift in obliquity.

[44] At first glance, it is clear that greater insolation at high obliquity will lead to warmer surface temperatures in the polar regions during the summer months. Additionally, the increased sublimation of surface ice at the poles will contribute a greater amount of water vapor to the atmosphere, increasing the warming effect. Conversely, at low obliquity, the poles remain in perpetual twilight or darkness and cold trap both atmospheric water and CO_2 . Figure 9 shows the annually averaged temperatures for an atmosphere at (a) 5°, (b) 15°, (c) 25°, (d) 45°, and (e) 60° obliquity, with SO_2 and a standard water cycle—all other model parameters are identical to those illustrated previously. Globally averaged surface temperatures are little changed through the obliquity cycle, as the mean distance to the Sun has not changed—this is expected.

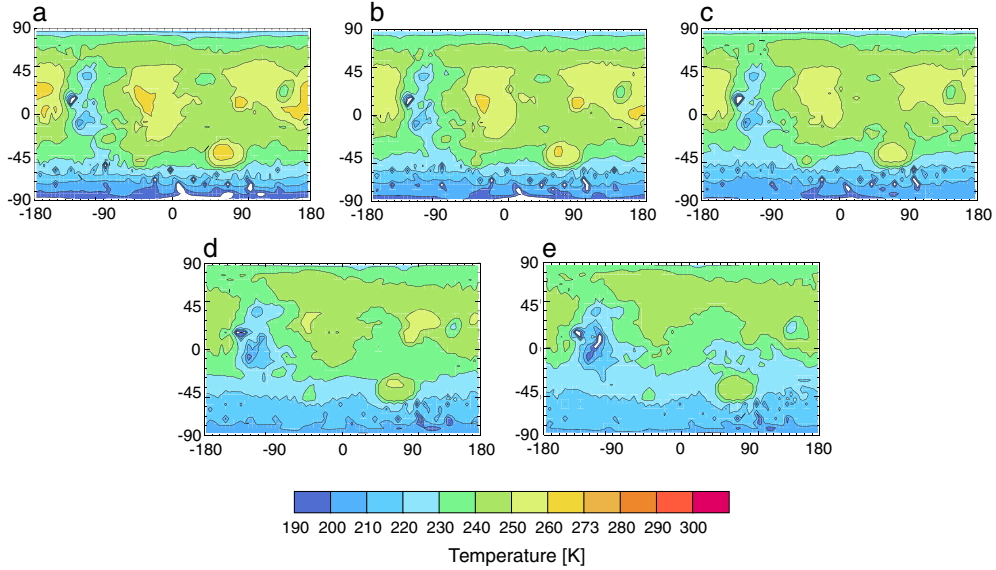


Figure 9. Annual average surface temperature for five obliquity values from 5° to 60° . (a) 5° , (b) 15° , (c) 25° , same as Figure 3e, (d) 45° , and (e) 60° . Atmosphere assumed to have a standard water cycle.

Peak temperatures are found in tropical latitudes during all obliquity periods, but in general, they become progressively cooler as obliquity increases. Global annual mean temperatures are listed in Table 1. Annual average temperatures are somewhat misleading however, as they, by their nature, average together the warmest summertime temperatures with the coldest winter nighttime temperatures. The result is an average temperature in the tropics that is still warmer than the mid and high latitudes but with a lower average saturation vapor pressure [Mischna et al., 2003]. This does not provide the full picture, however, and the viability of longer-term liquid water is perhaps better illustrated in Figure 10, which, again, illustrates the fraction of the martian year for which temperatures exceed 273 K (cf. Figure 4). Here, we see a dramatic rise in the occurrence of warm

temperatures in the north as obliquity rises, with a large swath of the northern hemisphere exceeding 273 K for more than 30% of the year. Much of this is in a single, contiguous summertime period where peak surface temperatures can reach as high as 300 K. Throughout the southern mid and high latitudes, temperatures are above this threshold for about 25% of the year. These are perhaps the most typical types of conditions we might expect on early Mars following volcanic activity with a subsaturated atmosphere, although we find no indication of perpetually warm conditions that might sustain liquid water indefinitely.

[45] We may try to maximize the possible warming found in the atmosphere by saturating the atmosphere, but even under these conditions (Figures 11 and 12), we find temperatures remaining below 273 K across the planet,

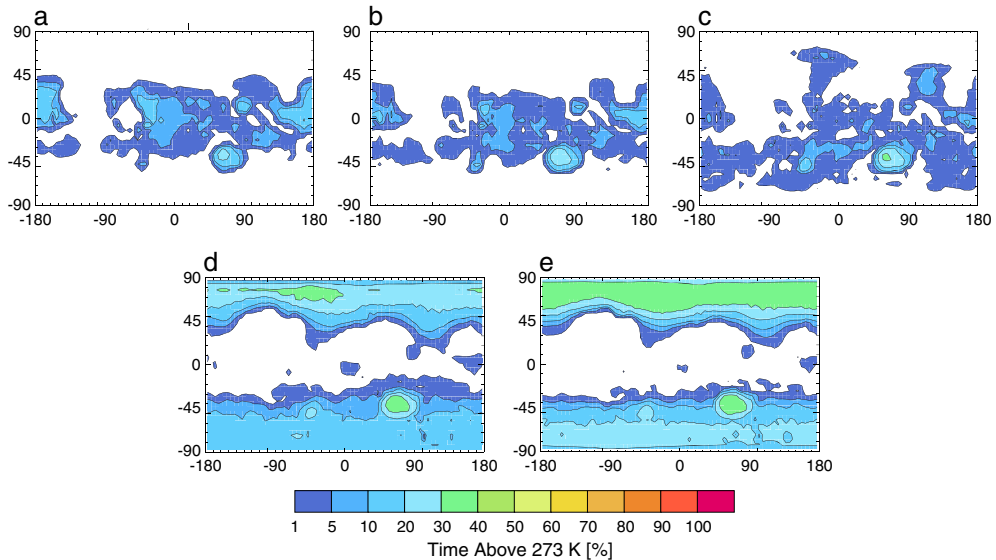


Figure 10. Fraction of the year for which surface temperatures exceed 273 K for the same simulations as in Figure 9.

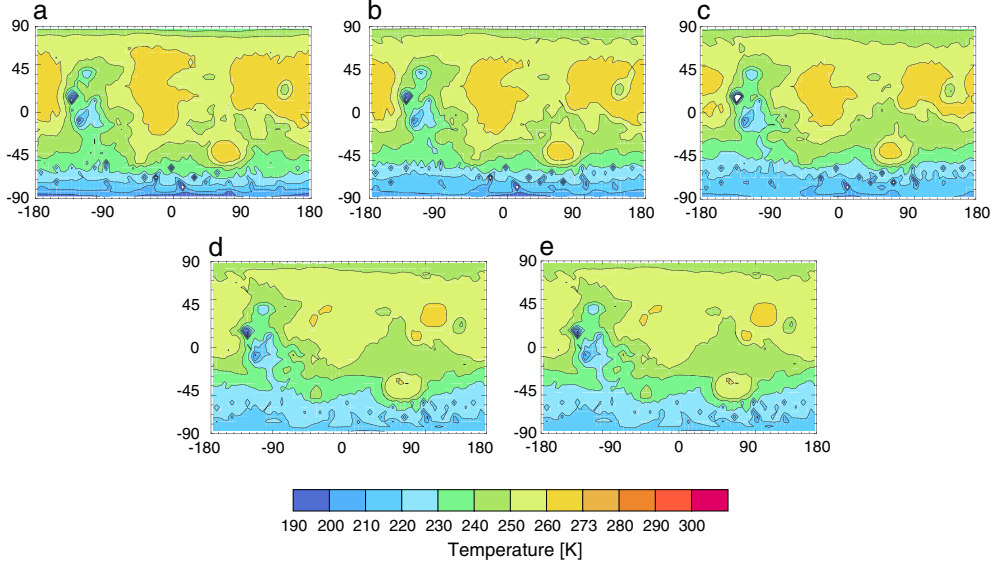


Figure 11. Same as Figure 9 but for a fully saturated atmosphere.

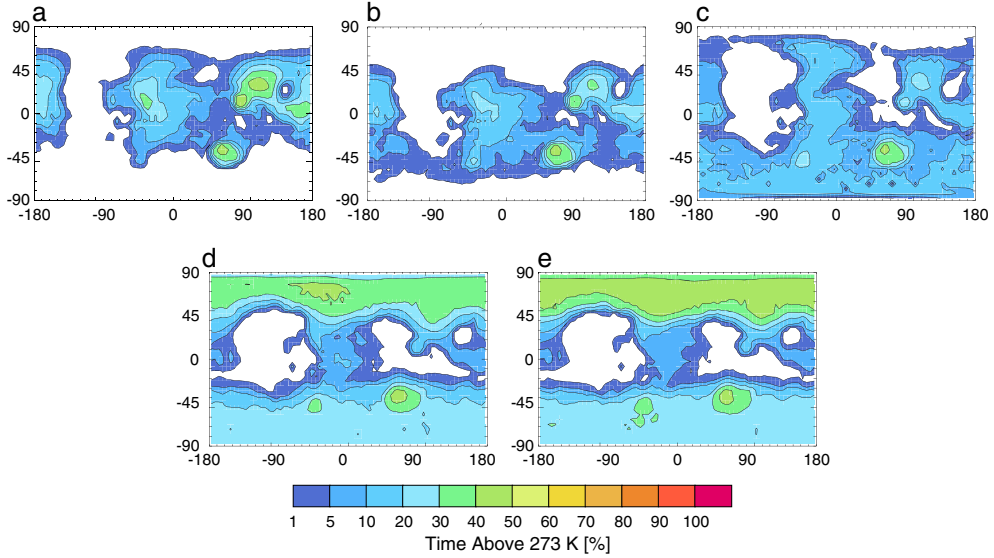


Figure 12. Same as Figure 10 but for a fully saturated atmosphere.

yielding locations in the northern mid and high latitudes that are above freezing for only about 50% of the year. This is sufficient, however, to allow for slow, year-by-year fluvial incision to produce the observed features, which do not require perpetually warm temperatures as a precondition for their development—only seasonal. Thicker baseline CO₂ pressures may compensate partially and provide some additional warming; however, thicker atmospheres are not favored later in martian evolution, e.g., during the Hesperian. The significantly increased duration over which warm temperatures are generated during periods of higher obliquity points to the necessary combination of trace gas injection and high obliquity for their formation.

[46] In the opposite direction (not shown), we find that the removal of the trace gas from the atmosphere causes a steady drop in temperature back to the initial, water-saturated value,

suggesting that upon loss of the trace gas, the system will return to its nominal state once again.

5.3. Water Sources

[47] To this point, we have overlooked the (necessary) condition of having a source for liquid water at the locations where we have identified warm temperatures, in order to explain they observed fluvial features. Two potential mechanisms for this water can be plausibly invoked and remain consistent with the present results. First, the source of the water may be surface deposits of ice that subsequently melt. While the location of many of the observed fluvial features is inconsistent with a planetary orientation similar to the present, during periods of higher obliquity, it would be possible to have water ice deposits put down in the tropics, as discussed in section 5.2. Over long periods, these

deposits could become substantially thick, possibly providing a periodic source for meltwater during the lower obliquity phases. During a subsequent obliquity excursion, the process would repeat, consistent with the complex history observed in the bedrock, which appears to require multiple episodes of erosion and incision to form terraced and layered deposits. Fluvial systems are much more widespread across the ancient highlands and crust than those originally observed by Viking, and the locations of warm temperatures that are found in Figures 9–12 are consistent with some but not all of the fluvial features observed at the surface; thus, we cannot conclusively dismiss or accept that meltwater is the sole mechanism for establishing liquid surface water.

[48] The second source of the water may arise from the subsurface as a result of large-scale, periodic volcanic activity. The originating phase of this water, then, would be liquid, leading to a different evolutionary development. This mechanism is consistent with the MEGAOUTFLO hypothesis discussed in section 2.2 and the periodic, obliquity-regulated warming episodes we observe in our simulations. Under MEGAOUTFLO, the “initial state” for the perturbed surface environment can begin with a substantial amount of liquid water rather than smaller trickles of surface melt. The subsequent greenhouse conditions produced by the elevated levels of volcanic gases (H_2O and trace gases included) would be able to sustain this liquid water for at least some time. This introduces a mechanism by which liquid water is made available to the surface—one that does not strictly require warm temperatures but, given such, can benefit by remaining liquid for extended periods, even through cold seasons when meltwater would not be produced.

5.4. Surface Properties

[49] The question of surface temperatures able to support liquid water (i.e., T roughly equal to or above 273 K) is, as we have seen, critically dependent on the amount of greenhouse warming, but it is also strongly controlled by the radiative properties of the surface itself. This latter point has thus far received much less attention than accorded to other forcing factors. The current albedo of Mars is determined by the local, relatively bright, dust cover fraction over a much darker (largely basaltic) surface. Dust cover lifts the albedo to about 0.25–0.35 whereas surface albedo can fall below 0.15 for minimally dusty regions. The presence of any dark material on the surface, such as unweathered basalt, or even liquid water can result in even lower surface albedos—open water on Earth exhibits an albedo as low as 8%.

[50] We cannot say with conviction what the surface properties of early Mars were, nor is it clear what the long-term weathering profile of the exposed surface material was. Certainly, it is plausible that aeolian erosion has been a consistent player on Mars since its earliest days, leading to dusty (and, by extension, bright) conditions since the Noachian. However, it is at least equally plausible that on early Mars, with a warmer, thicker, potentially more humid atmosphere and a shorter geologic period over which aeolian erosion would have taken place, the surface was less physically weathered with a brightness significantly lower than the present day. Further, the level of chemical weathering of surface basalt is uncertain on early Mars. Chemical weathering of basalt tends to form palagonite, clays, zeolites, and other amorphous forms in addition to iron oxides (e.g., hematite),

which tend to appear brighter than the source material. However, in the absence of an oxidizing atmosphere, oxidative weathering will be suppressed, and the formation of many forms of bright material will be minimized. While Meridiani Planum shows widespread formation of hematite dated to the Noachian/Hesperian boundary, no widespread evidence of iron oxides has been found in more ancient, Noachian, terrains.

[51] To test the sensitivity to surface properties, particularly albedo, a set of simulations adjusting surface parameters in various combinations was run. Beginning with a simulation having a standard water cycle and SO_2 (Figures 13a and 14a), two further simulations (Figures 13b and 13c and 14b and 14c) were performed, but with the northern hemisphere (only) albedo changed to 0.12 and 0.08, respectively. The goal is to crudely approximate the dark appearance of an early Mars surface in the north. It is shown that with the surface brightness reduced, much of the northern hemisphere is able to maintain temperatures at or above freezing for much or all of the year.

[52] While a simple, dark basaltic surface is consistent with the aforementioned model simulations, it is enticing to ponder the possibility that the “dark” surface modeled in the northern hemisphere could, in fact, be that of liquid water. Were this the case, the atmosphere would be more humid than the standard water cycle simulations would suggest—perhaps being closer to saturated conditions. Figures 13d and 14d show annual average temperatures and the fraction of the year >273 K for a saturated atmosphere having SO_2 and with a northern hemisphere surface albedo of 0.08. Areas with the greatest fraction of time above freezing (>90% in Figure 14d) generally conform to areas with the greatest thermal inertia (the thermal inertia distribution used in these simulations is the same as for the present day). Areas of high thermal inertia would be able to maintain warm temperatures for longer periods if the initial state were, itself, warm. Whether an ocean or a dry,

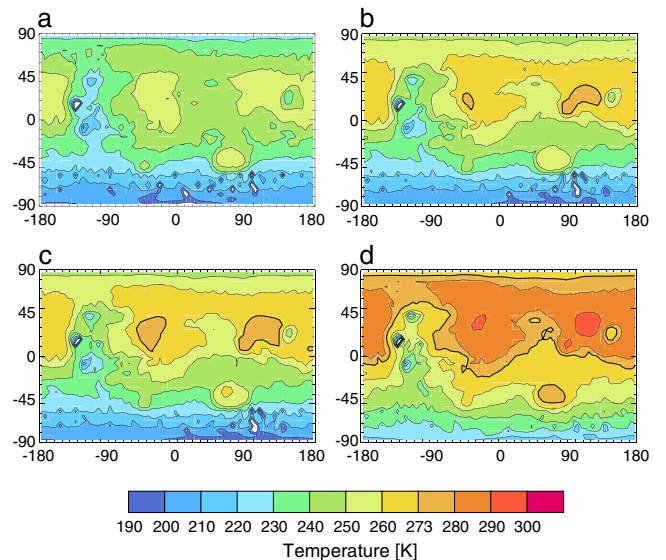


Figure 13. Annual average temperatures for surface property simulations with standard water cycle and with northern hemisphere prescribed a different, fixed albedo, (a) standard case (cf. Figure 3e); (b) northern hemisphere albedo 0.12; (c) northern hemisphere albedo 0.08; (d) northern hemisphere albedo 0.08 with saturated atmosphere.

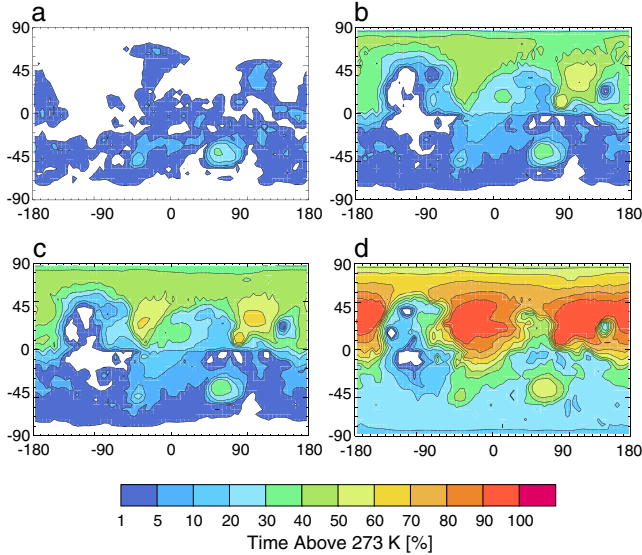


Figure 14. Same conditions as Figure 13 but for fraction of year with temperatures $>273\text{ K}$.

dark surface, the argument remains the same, although for the former, the presence of a phase-changing substance does present some additional complexities.

[53] It has recently been recognized that the geomorphology of valley networks in the southern Mars highlands implies significant episodes of rainfall for their genesis [Craddock and Howard, 2002; Barnhart et al., 2009; Hoke et al., 2011]. Moreover, much of the network development occurred during a relatively brief episode of martian history around the time of the Noachian/Hesperian boundary [Howard et al., 2005; Irwin et al., 2005; Mangold et al., 2012].

[54] It is also observed that the spatial distribution of the valley networks is not uniform, as might be expected if, for example, impacts into the southern highlands were responsible for episodic formation of the networks [Toon et al., 2010]. Instead, the distribution is consistent with what would be expected for a precipitation source associated with a northern plains ocean [Luo and Stepinski, 2009; Stepinski and Luo, 2010]. This relationship of valleys to the margins of the northern edge of the heavily cratered terrain of the southern highlands has been confirmed by an independent study that quantified the spatial distribution of drainage densities [Hynek et al., 2010]. The distribution also corresponds to the locations of deltas that are graded to the base level of a northern plains ocean [DiAchille and Hynek, 2010], to the concentrations of sedimentary rocks on Mars [Malin and Edgett, 2000; Delano and Hynek, 2011], and to the presence of high-Al clay minerals in deep weathering profiles [Le Deit et al., 2012; Loizeau et al., 2012]. The latter would require intense leaching in a surficial environment for their formation. Moreover, such a leaching episode would occur at the Noachian/Hesperian boundary [Loizeau et al., 2012], corresponding to the same episode of precipitation recognized in regard to the valley networks.

[55] Fairén et al. [2012] have explored the ramifications of a dark, near-global surface ocean on early Mars with a 0-D energy balance model derived from the work of Williams and Kasting [1997]. Their conclusions indicate that it becomes difficult to obtain warm ($>273\text{ K}$) global temperatures for all but the most globally ocean-covered scenarios,

even with a 3 bar CO_2 atmosphere. For most situations, global temperatures remain below freezing. To this end, our model agrees with their findings, as our global temperatures do not ever exceed 273 K (Table 1), and even with a dark, global ocean and a 3 bar CO_2 atmosphere (not shown), our globally, annually averaged temperatures never exceed 243 K (cf. 228.8 K at 500 mb); however, as we have noted, this does not preclude the possibility of periodic and localized warm conditions, which appear widespread in our 3-D model and which cannot be reproduced in an energy balance model. There are multiple reasons that the ability to obtain warm conditions appears not to be as dire as suggested by Fairén et al. [2012] and by the global average values in our model. First, in the aforementioned study, heat transport is modeled with a simplified diffusion parameterization, which neglects the true atmospheric circulation, which we find important. Second, the Fairén et al. [2012] radiative transfer scheme neglects the important radiative heating from SO_2 or other trace gases, which, as we find, contributes non-negligible warming to the atmosphere.

[56] In summary, surface albedo and thermal inertia are crucial, but largely overlooked, aspects of ancient martian climate. Simple calculations suggest the plausibility of a dark, high thermal inertia surface sustaining warm temperatures for prolonged periods. There may be multiple origins of this putative dark surface, and we have presented evidence that suggests that large surface water deposits, potentially emplaced during warmer phases in martian history, are not inconsistent with the amount of warming observed in our climate model studies nor is the presence of large deposits of unweathered, dry, basaltic material. Further work is needed, but any declaration of Mars being cold and dry on the basis of climate model results alone is probably premature.

6. Discussion

[57] The results shown here contrast strongly with recent results from Johnson et al. [2008] and do not show widespread global warming introduced by the presence of water vapor and SO_2 in the martian atmosphere. Rather, such warming may be found in localized environments for relatively short periods of time. Nevertheless, the behavior of the climate system is consistent with one for which the water cycle is influenced by the orbital cycles of the planet. We specifically note two things. First, the water cycle has a markedly different nature between low and high obliquities, as expected. As obliquity decreases, the level of atmospheric water vapor drops precipitously, and the atmosphere is incapable of sustaining warm temperatures in all but the most limited tropical regions for the shortest of periods. In brief, we cannot expect conditions conducive to stable liquid water anywhere, even in the presence of IR-active trace gases such as SO_2 .

[58] Second, we note that the role of a trace gas “trigger” is a necessary component of this model, without which, the system never gets sufficiently warm to initiate widespread sublimation from the extant polar caps (or surface liquid water reservoirs). As obliquity rises (Figure 14), and the atmosphere becomes more humid, temperatures will rise globally. In the absence of other trace gases, the warming influence of water vapor alone is quite moderate and the surface rarely exceeds the 273 K threshold. More specifically,

even in those circumstances when it does, there will be insufficient water vapor in the atmosphere to produce a greenhouse effect large enough to maintain warm temperatures through the diurnal cycle. Nighttime temperatures are cool, and much of the daytime water vapor is lost, reducing the greenhouse warming even further.

[59] Conversely, in the presence of a trace gas such as SO₂, the overall warming, particularly in the warmest locations, is elevated to a point where even during the nighttime hours, it may remain high enough to support elevated levels of water vapor, and the warm temperatures are maintained throughout the day. Thus, it seems that three components are necessary to invoke a global climate conducive to large-scale warmth—volcanic activity that releases an IR-active trace gas such as SO₂, a significantly humid atmosphere to provide ample warming, and high obliquity to enable periods of long-term warming.

[60] The idea of a darker surface is an interesting one that deserves future study. Our initial simulations reveal significant warming with the presence of a darker surface globally. It seems necessary in our modeling system to decrease the planetary albedo in order to obtain perpetually warm temperatures in this greenhouse atmosphere. As mentioned previously, the same general conditions can be reached by invoking a dark liquid water ocean or by assuming the widespread presence of low-albedo rock. The ubiquitous presence of Fe-oxide-bearing dust on the surface of Mars is likely an evolving feature, and in Mars' early history, there may have been significantly less dust on the surface due to a reduced period in which such fine-grained, bright material could have accumulated. Further, in a more humid environment, the accumulation and aeolian transport of unconsolidated dust would likely be less due to greater precipitation, increased cementation of dust, and sedimentation within any bodies of standing water. Or, more simply put, dust and other fine-grained materials may have had a greater probability of becoming part of the rock record as opposed to remaining as unconsolidated sediment.

[61] In conclusion, it seems difficult to generate widespread surface warming in a CO₂+H₂O+SO₂ atmosphere of any plausible composition, although seasonal warming is found across much of the surface, for at least brief periods, and in some locations for a significant fraction of the Mars year. Warm conditions can be further enhanced by the presence of a darker surface than the present day. Such periodic warming is, as we have discussed in section 2, wholly consistent with both the geochemical [Milliken et al., 2008] and geomorphological [Mangold et al., 2004, 2008] record during the Hesperian, which indicates only periodic, but not perpetual, warming. Changes in obliquity do provide modest changes in the likelihood of surface water due in large part to the increase in water vapor content introduced by the exposure of the polar caps. This warming is triggered by the presence of a trace gas such as SO₂ and modulated by the oscillations in the obliquity cycle. In the absence of any of these three components (available water vapor, trace gas trigger, and high obliquity), the cycle does not perpetuate. We have intentionally neglected some significant negative feedback mechanisms in the present work—most specifically the existence of water clouds and sulfur aerosols in the atmosphere—both of which may have a significant cooling effect on overall climate. The difficulty with which warm conditions are obtained under

the more “standard” simulations without any such cooling effects makes the likelihood of obtaining surface water ever more challenging if such factors are incorporated. In this way, our simulations provide perhaps very optimistic estimates for the plausibility of liquid water on Mars. Future work should continue to examine the role of atmospheric clouds and aerosols and more deeply explore the possible role of a northern ocean on early Mars.

[62] **Acknowledgments.** Resources supporting this work were provided by the NASA High-End Computing Program through the NASA Advanced Supercomputing Division at Ames Research Center as well as from the JPL Office of the Chief Information Officer. MAM, VB, RM, and CL were supported by a NASA Mars Fundamental Research Program grant NNH10ZDA001N to JPL. Additional support for CL and MIR was provided by a NASA Planetary Atmospheres grant NNX10AB42G to Ashima Research. Part of this research was carried out at the Jet Propulsion Laboratory, California Institute of Technology, under a contract with the National Aeronautics and Space Administration.

References

- Baker, V. R. (2001), Water and the martian landscape, *Nature*, **412**, 228–236.
- Baker, V. R. (2009), Megafloods and global paleoenvironmental change on Mars and Earth, in *Preservation of Random Megascalar Events on Mars and Earth: Influence on Geologic History*, Geological Society of America Special Paper 453, edited by M. G. Chapman, and L. Keszthelyi, pp. 25–36, doi:10.1130/2009.453(03).
- Baker, V. R., and J. Partridge (1986), Small martian valleys: Pristine and degraded morphology, *J. Geophys. Res.*, **91**, 3561–3572.
- Baker, V. R., R. G. Strom, V. C. Gulick, J. S. Kargel, G. Komatsu, and V. S. Kale (1991), Ancient oceans, ice sheets and hydrological cycle on Mars, *Nature*, **352**, 589–594.
- Barnhart, C. J., A. D. Howard, and J. M. Moore (2009), Long-term precipitation and late-stage valley network formation: Landform simulations of Paraná Basin, Mars, *J. Geophys. Res.*, **114**, E01003, doi:10.1029/2008JE003122.
- Bibring, J.-P., et al. (2006), Global mineralogical and aqueous Mars history derived from OMEGA/Mars Express data, *Science*, **312**, 400–404.
- Bradley, B. A., S. E. H. Sakimoto, H. Frey, and J. R. Zimbelman (2002), Medusa Fossae Formation: New perspectives from Mars Global Surveyor, *J. Geophys. Res.*, **107**, doi:10.1029/2001JE001537.
- Carr, M. H. (1996), Water on Mars, 229 pp., Oxford University Press, New York.
- Carter, J., F. Poulet, J.-P. Bibring, and S. Murchie (2010), Detection of hydrated silicates in crustal outcrops in the northern plains of Mars, *Science*, **328**, 1682–1686.
- Christensen, P. R. (2003), Formation of recent martian gullies through melting of extensive water-rich snow deposits, *Nature*, **422**, 45–58.
- Christensen, P. R., et al. (2001), Mars Global Surveyor Thermal Emission Spectrometer experiment: Investigation description and surface science results, *J. Geophys. Res.*, **106**, 23,823–23,871.
- Clark, B. C., and D. C. Van Hart (1981), The salts of Mars, *Icarus*, **45**, 370–378.
- Clifford, S. M., and T. J. Parker (2001), The evolution of the martian hydrosphere: Implications for the fate of a primordial ocean and the current state of the northern plains, *Icarus*, **154**, 40–79.
- Craddock, R. A., and A. D. Howard (2002), The case for rainfall on a warm, wet early Mars, *J. Geophys. Res.*, **107**(E11), 5111, doi:10.1029/2001JE001505.
- Delano, K., and B. M. Hynek (2011), Intracrater layered deposits support ancient ocean on Mars, 42nd Lunar and Planetary Science Conference, held March 7–11, 2011 at The Woodlands, Texas. LPI Contribution No. 1608, 2636 pp.
- DiAchille, G., and B. M. Hynek (2010), Ancient ocean on Mars supported by global distribution of deltas and valleys, *Nat. Geosci.*, **3**, 459–463.
- Edwards, J. M., and A. Slingo (1996), Studies with a flexible new radiation code, I: Choosing a configuration for a large-scale model, *Quart. J. R. Meteorol. Soc.*, **122**, 689–719.
- Ehlmann, B. L., J. F. Mustard, S. L. Murchie, J.-P. Bibring, A. Meunier, A. A. Fraeman, Y. Langevin (2011), Subsurface water and clay mineral formation during the early history of Mars, *Nature*, **479**, 53–60.
- Fairén, A. G., J. D. Haqq-Misra, and C. P. McKay (2012), Reduced albedo on early Mars does not solve the climate paradox under a faint young Sun, *Astron. Astrophys.*, **540**, doi:10.1051/0004-6361/201118527.
- Forget, F., and R. T. Pierrehumbert (1997), Warming early Mars with carbon dioxide clouds that scatter infrared radiation, *Science*, **278**, 1273–1276.

- Forget, F., R. M. Haberle, F. Montmessin, B. Levrard, and J. W. Head (2006), Formation of glaciers on Mars by atmospheric precipitation at high obliquity, *Science*, **311**, 368–371.
- Forget, F., R. Wordsworth, E. Millour, J.-B. Madeleine, L. Kerber, J. Leconte, E. Marcq, and R. M. Haberle (2013), 3D modeling of the early martian climate under a denser CO₂ atmosphere: Temperatures and CO₂ ice clouds, *Icarus*, **222**, 81–99.
- Fu, Q., and K. N. Liou (1992), On the correlated k-distribution method for radiative transfer in nonhomogeneous atmospheres, *J. Atmos. Sci.*, **49**, 2139–2156.
- Gough, D. O. (1981), Solar interior structure and luminosity variations, *Solar Phys.*, **74**, 21–34.
- Gulick, V. (2001), Origin of the valley networks on Mars: A hydrological perspective, *Geomorphology*, **37**, 241–268.
- Guo, X., W. G. Lawson, M. I. Richardson, and A. Toigo (2009), Fitting the Viking lander surface pressure cycle with a Mars General Circulation Model, *J. Geophys. Res.*, **114**, E07006, doi:10.1029/2008JE003302.
- Haberle, R. M., J. R. Murphy, and J. Schaeffer (2003), Orbital change experiments with a Mars general circulation model, *Icarus*, **161**, 66–89.
- Halevy, I., M. T. Zuber, and D. P. Schrag (2007), A sulfur dioxide climate feedback on early Mars, *Science*, **318**, 1903–1907.
- Halevy, I., R. T. Pierrehumbert, and D. P. Schrag (2009), Radiative transfer in CO₂-rich paleoatmospheres, *J. Geophys. Res.*, **114**, D18112, doi:10.1029/2009JD011915.
- Halevy, I., W. W. Fischer, and J. M. Eiler (2011), Carbonates in the martian meteorite Allan Hills 84001 formed at 18 ± 4 °C in a near-surface aqueous environment, *Proc. Natl. Acad. Sci.*, **108**, doi:10.1073/pnas.1109444108.
- Head, J. W., J. F. Mustard, M. A. Kreslavsky, R. E. Milliken, and D. R. Marchant (2003), Recent ice ages on Mars, *Nature*, **426**, 797–802.
- Head, J. W., et al. (2005), Tropical to mid-latitude snow and ice accumulation, flow and glaciation on Mars, *Nature*, **434**, 346–351.
- Hecht, M. H., et al. (2009), Detection of perchlorate and the soluble chemistry of martian soil at the Phoenix landing site, *Science*, **325**, 64–67.
- Hoke, M. R. T., and B. M. Hynek (2009), Roaming zones of precipitation on ancient Mars as recorded in valley networks, *J. Geophys. Res.*, **114** (E08002), doi:10.1029/2008JE003247.
- Hoke, M. R. T., G. Tucker, and B. M. Hynek (2011), Formation timescales of large Martian valley networks, *Earth Planet. Sci. Lett.*, **312**, 1–12.
- Howard, A. D., J. M. Moore, and R. P. Irwin, III (2005), An intense terminal epoch of widespread fluvial activity on early Mars: 1. Valley network incision and associated deposits, *J. Geophys. Res.*, **110**, E12S14, doi:10.1029/2005JE002459.
- Hynek, B. M., M. Beach, and M. R. T. Hoke (2010), Updated global map of Martian valley networks and implications for climate and hydrologic processes, *J. Geophys. Res.*, **115**, E09008, doi:10.1029/2009JE003548.
- Irwin, R. P. III, A. D. Howard, R. A. Craddock, and J. M. Moore (2005), An intense terminal epoch of widespread fluvial activity on early Mars: 2. Increased runoff and paleolake development, *J. Geophys. Res.*, **110**, E12S15, doi:10.1029/2005JE002460.
- Jakosky, B. M., and M. H. Carr (1985), Possible precipitation of ice at low latitudes of Mars during periods of high obliquity, *Nature*, **315**, 559–561.
- Johnson, S. S., M. A. Mischna, T. L. Grove, and M. T. Zuber (2008), Sulfur-induced greenhouse warming on early Mars, *J. Geophys. Res.*, **113**, E08005, doi:10.1029/2007JE002962.
- Johnson, S. S., A. A. Pavlov, and M. A. Mischna (2009), Fate of SO₂ in the ancient martian atmosphere: Implications for transient greenhouse warming, *J. Geophys. Res.*, **114**, E11011, doi:10.1029/2008JE003313.
- Kasting, J. F. (1982), Stability of ammonia in the primitive terrestrial atmosphere, *J. Geophys. Res.*, **87**, 3091–3098.
- Kasting, J. F. (1991), CO₂ condensation and the climate of early Mars, *Icarus*, **94**, 1–13.
- King, P. L., and S. M. McLennan (2010), Sulfur on Mars, *Elements*, **6**, doi:10.2113/gselements.6.2.107.
- Kuhn, W. R., and S. K. Atreya (1979), Ammonia photolysis and the greenhouse effect in the primordial atmosphere of the Earth, *Icarus*, **37**, 207–213.
- Lacis, A. A., and V. Oinas (1991), A description of the correlated k-distribution method for modeling nongray gaseous absorption, thermal emission, and multiple scattering in vertically inhomogeneous atmospheres, *J. Geophys. Res.*, **96**, 9027–9074.
- Laskar, J., M. Gastineau, F. Joutel, P. Robutel, B. Levrard, and A. Correia (2004), Long term evolution and chaotic diffusion of the insolation quantities of Mars, *Icarus*, **170**, 343–364.
- Le Deit, L., J. Flahaut, C. Quantin, E. Hauber, D. Mège, O. Bourgeois, J. Gurgurewicz, M. Massé, and R. Jaumann (2012), Extensive surface pedogenic alteration of the Martian Noachian crust suggested by plateau phyllosilicates around Valles Marineris, *J. Geophys. Res.*, **117**, E00J05, doi:10.1029/2011JE003983.
- Limaye, A., O. Aharonson, and J. T. Perron (2012), Detailed stratigraphy and bed thickness of the Mars north and south polar layered deposits, *J. Geophys. Res.*, **117**, E06009.
- Loizeau, D., S. C. Werner, N. Mangold, J.-P. Bibring, and J. L. Vago (2012), Chronology of deposition and alteration in the Mawrth Vallis region, Mars, *Planet. Space Sci.*, doi:10.1016/j.pss.2012.06.023.
- Luo, W., and T. F. Stepinski (2009), Computer-generated global map of valley networks on Mars, *J. Geophys. Res.*, **114**, E11010, doi:10.1029/2009JE003357.
- Malin, M. C., and K. S. Edgett (2000), Sedimentary rocks of early Mars, *Science*, **290**, 1927–1937.
- Mangold, N., C. Quantin, V. Ansan, C. Delacourt, and P. Allemand (2004), Evidence for precipitation on Mars from dendritic valleys in the Valles Marineris area, *Science*, **305**, 78–81.
- Mangold, N., V. Ansan, P. Masson, C. Quantin, and G. Neukum (2008), Geomorphic study of fluvial landforms on the northern Valles Marineris plateau, Mars, *J. Geophys. Res.*, **113**, E08009.
- Mangold, N., S. Adeli, S. Conway, V. Ansan, and B. Langlais (2012), A chronology of early Mars climatic evolution from impact crater degradation, *J. Geophys. Res.*, **117**, E00405, doi:10.1029/2011JE004005.
- McLennan, S. M., and J. P. Grotzinger (2008), The sedimentary rock cycle of Mars, in *The Martian Surface – Composition, Mineralogy, and Physical Properties*, edited by J. F. Bell, pp. 541–577, Cambridge University Press, Cambridge.
- Michalakes, J., J. Dudhia, D. Gill, T. Henderson, J. Klemp, W. Skamarock, and W. Wang (2004), The weather research and forecast model: Software architecture and performance, in *Proceedings of the 11th ECMWF Workshop on the Use of High Performance Computing In Meteorology*, edited by G. Mozdzynski, pp. 156–168, Eur. Cent. for Medium-Range Weather Forecasts, Reading, U.K.
- Milkovich, S. M., and J. W. Head, III (2005), North polar cap of Mars: Polar layered deposit characterization and identification of a fundamental climate signal, *J. Geophys. Res.*, **110**, E01005, doi:10.1029/2004JE002349.
- Milliken, R. E., et al. (2008), Opaline silica in young deposits on Mars, *Geology*, **36**, 847–850.
- Milliken, R. E., J. F. Mustard, and D. L. Goldsby (2003), Viscous flow features on the surface of Mars: Observations from high-resolution Mars Orbiter Camera (MOC) images, *J. Geophys. Res.*, **108**(E6), doi:10.1029/2002JE002005.
- Mischna, M. A., J. F. Kasting, A. Pavlov, and R. Freedman (2000), Influence of carbon dioxide clouds on early martian climate, *Icarus*, **145**, 546–554.
- Mischna, M. A., M. I. Richardson, R. J. Wilson, and D. J. McCleese (2003), On the orbital forcing of Martian water and CO₂ cycles: A general circulation model study with simplified volatile schemes, *J. Geophys. Res.*, **108**(E6), 5062, doi:10.1029/2003JE002051.
- Mischna, M. A., and M. I. Richardson (2005), A reanalysis of water abundances in the martian atmosphere at high obliquity, *Geophys. Res. Lett.*, **32**, L03201, doi:10.1029/2004GL021865.
- Mischna, M. A., C. Lee, and M. I. Richardson (2012), Development of a fast, accurate radiative transfer model for the martian atmosphere, past and present, *J. Geophys. Res.*, **117**, E10009, doi:10.1029/2012JE004110.
- Mustard, J. F., C. D. Cooper, and M. K. Rifkin (2001), Evidence for recent climate change on Mars from the identification of youthful near-surface ground ice, *Nature*, **412**, 411–414.
- Neukum, G., et al. (2004), Recent and episodic volcanic and glacial activity on Mars revealed by the High Resolution Stereo Camera, *Nature*, **432**, 971–979.
- Plaut, J. J., A. Safaeinili, J. W. Holt, R. J. Phillips, J. W. Head, R. Seu, N. E. Putzig, and A. Frigeri (2009), Radar evidence for ice in lobate debris aprons in the mid-northern latitudes of Mars, *Geophys. Res. Lett.*, **36**, L02203, doi:10.1029/2008GL036379.
- Pollack, J. B., J. F. Kasting, S. M. Richardson, and K. Poliakoff (1987), The case for a warm wet climate on early Mars, *Icarus*, **71**, 203–224.
- Postawko, S. E., and W. R. Kuhn (1986), Effect of the greenhouse gases (CO₂, H₂O, SO₂) on martian paleoclimate, *J. Geophys. Res.*, **91**, D431–D438.
- Poulet, F., J.-P. Bibring, J. F. Mustard, A. Gendrin, N. Mangold, Y. Langevin, R. E. Arvidson, B. Gondet, C. Gomez, and the OMEGA Team (2005), Phyllosilicates on Mars and implications for early martian climate, *Nature*, **438**, 623–627.
- Putzig, N. E., M. T. Mellon, K. A. Kretke, and R. E. Arvidson (2005), Global thermal inertia and surface properties of Mars from the MGS mapping mission, *Icarus*, **173**, 325–341.
- Richardson, M. I., A. D. Toigo, and C. E. Newman (2007), PlanetWRF: A general purpose, local to global numerical model for planetary atmospheric and climate dynamics, *J. Geophys. Res.*, **112**, E09001, doi:10.1029/2006JE002825.
- Sackmann, I. J., and A. I. Boothroyd (2003), Our Sun. V. A bright young Sun consistent with helioseismology and warm temperatures on ancient Earth and Mars, *Ap. J.*, **583**, 1024–1039.
- Sagan, C., and C. Chyba (1997), The early faint Sun paradox: Organic shielding of ultraviolet-labile greenhouse gases, *Science*, **276**, 1217–1221.

- Segura, T. L., O. B. Toon, A. Colaprete, and K. Zahnle (2002), Environmental effects of large impacts on Mars, *Science*, 298, 1977–1980.
- Segura, T. L., O. B. Toon, and A. Colaprete (2008), Modeling the environmental effects of moderate-sized impacts on Mars, *J. Geophys. Res.*, 113, E11007, doi:10.1029/2008JE003147.
- Skamarock, W. C., J. B. Klemp, J. Dudhia, D. O. Gill, D. M. Barker, W. Wang, and J. G. Powers (2005), A description of the Advanced Research WRF Version 2, NCAR Tech. Note 468+STR, Natl. Cent. for Atmos. Res., Boulder, Colo.
- Skamarock, W. C., and J. B. Klemp (2008), A time-split nonhydrostatic atmospheric model for weather research and forecasting applications, *J. Comp. Phys.*, 227, 3465–3485.
- Squyres, S. W., and J. F. Kasting (1994), Early Mars: How warm and how wet?, *Science*, 265, 744–749.
- Stepinski, T. F., and W. Luo (2010), Global pattern of dissection on Mars and the northern ocean hypothesis, 41st Lunar and Planetary Science Conference, The Woodlands, Texas, March 1–5, 2010. LPI Contribution No. 1533, 1350 pp.
- Tian, F., M. W. Claire, J. D. Haqq-Misra, M. Smith, D. C. Crisp, D. Catling, K. Zahnle, and J. F. Kasting (2010), Photochemical and climate consequences of sulfur outgassing on early Mars, *Earth Planet. Sci. Lett.*, 295, 412–418.
- Toon, O. B., T. Segura, and K. Zahnle (2010), The formation of martian river valleys by impacts, *Ann. Rev. Earth Planet. Sci.*, 38, 303–322.
- Tosca, N. J., and A. H. Knoll (2009), Juvenile chemical sediments and the long term persistence of water at the surface of Mars, *Earth Planet. Sci. Lett.*, 286, 379–386.
- Werner, S. C. (2009), The global martian volcanic evolutionary history, *Icarus*, 201, 44–68.
- Williams, D. M., and J. F. Kasting (1997), Habitable planets with high obliquities, *Icarus*, 129, 254–267.
- Wilson, L., and J. W. Head, III (2002), Tharsis-radial graben systems as the surface manifestation of plume-related dike intrusion complexes: Models and implications, *J. Geophys. Res.*, 107, 5057, doi:10.1029/2001JE001593.
- Wordsworth, R., F. Forget, and V. Eymet (2010), Infrared collision-induced and far-line absorption in dense CO₂ atmospheres, *Icarus*, 210, 992–997.
- Wordsworth, R., F. Forget, E. Millour, J. W. Head, J.-B. Madelaine, and B. Charnay (2013), Global modeling of the early martian climate under a denser CO₂ atmosphere: Water cycle and ice evolution, *Icarus*, 222, 1–19.
- Yung, Y. L., H. Nair, and M. F. Gerstell (1997), CO₂ greenhouse in the early martian atmosphere: SO₂ inhibits condensation. *Icarus*, 130, 222–224.